Geothermal Potential of the Kigluaik Fault System, Western Alaska: Structural Controls, Multicomponent Geothermometry, and Low-Temperature Thermochronology

Jason W. Craig,[1] Elizabeth L. Miller,[1] Jeff A Benowitz,[2] Max Manson,[1] and Carl W. Hoiland[3]

[1] Department of Earth and Planetary Sciences, Stanford University, Stanford, CA 94305-2115

[2] GeoSep Services, Moscow, Idaho 83843, USA

[3] Zanskar Geothermal & Minerals, Inc., Salt Lake City, UT 84101

Keywords

Alaska, Seward Peninsula, Nome, geothermal, structure, exploration, fault, thermochronology

ABSTRACT

Remote communities of the Seward Peninsula, Alaska, lack reliable forms of energy that are not derived from costly fossil fuels (>$7 gallon of diesel). Development of geothermal resources would provide reliable baseload power to the region. Prior geothermal exploration has focused on Pilgrim Hot Springs, but multiple drilling efforts have not yet fully characterized the geothermal system. Pilgrim Hot Springs is located ~5 km north of the Kigluaik Mountains, which is an active normal fault system not previously evaluated as a control for geothermal activity. This study assesses the Kigluaik fault system as a structural control for blind geothermal systems through the application of zircon and apatite (U-Th)/He low temperature thermochronology. Thermochronology from rocks along the surface trace of normal faults is a favorable means for discovering areas with blind hydrothermal activity. Applying this method is a novel and cost-effective tool for geothermal exploration of normal fault systems that would otherwise require costly and impactful approaches to probe a normal fault for the presence of geothermal activity by drilling. Samples collected along the trace of the Kigluaik fault system primarily yield 40-25 Ma apatite (U-Th)/He dates, with two samples yielding anonymously young (13 Ma) dates. Areas with anomalously young dates coincide with fault stepovers and intersections along the Kigluaik fault system and indicate zones with potential for hosting blind geothermal systems. Thermochronology results do not indicate that Pilgrim Hot Spring is directly controlled by the Kigluaik fault system. A concealed fault within the basin at a high angle to the Kigluaik fault is likely the primary structure controlling upflow at Pilgrim Hot Springs. GeoT multicomponent geothermometry yields 136.5°C estimates for Pilgrim Hot Springs and confirms prior conclusions that the region contains moderate temperature geothermal systems that could be economic sources of renewable power.

1. Introduction

Nome is an isolated community on the southwestern edge of the Seward Peninsula (Fig. 1), western Alaska, that relies on diesel-burning generators with minor contributions from wind turbines. Development of reliable and affordable energy in this region is crucial to sustain basic infrastructure and avoid fuel cost related community economic decline (Berman, 2017). Currently, options for energy in northern Alaska that are not derived from fossil fuels are limited. Development of a geothermal resource would provide reliable baseload power to the region with a reduced long-term environmental impact. Application of advanced geothermal exploration strategies may enable successful characterization and targeting of Alaska's geothermal resources and reignite exploration interest across the state.

Pilgrim Hot Springs (PHS) lies ~ 5 km north of the Kigluaik Mountains (Fig. 1), ~ 60 miles north of Nome, and has been the focus of geothermal exploration since the 1970's. The surface expression of PHS includes a series of hot pools (60-75˚C), lack of permafrost, and anomalous vegetation (Haselwimmer et al., 2013). The geologic controls for PHS are unclear and have been proposed to be related to radiogenic heat produced by Cretaceous plutons (Miller, 1994; Kolker, 2008), Quaternary magmatism (Till et at., 2011), or amagmatic fault-controlled hydrothermal circulation (e.g., Curewitz and Karson, 1997). The geothermal fluids are saline alkali-chloride springs; however, they have a documented $^{3}He/^{4}He$ ratio of Ra=0.9 (Liss and Motyka, 1994), which is a lower value for a mantle ^{3}He contribution than is expected for a mantle-derived magmatic heat source (Rizzo et al., 2022).

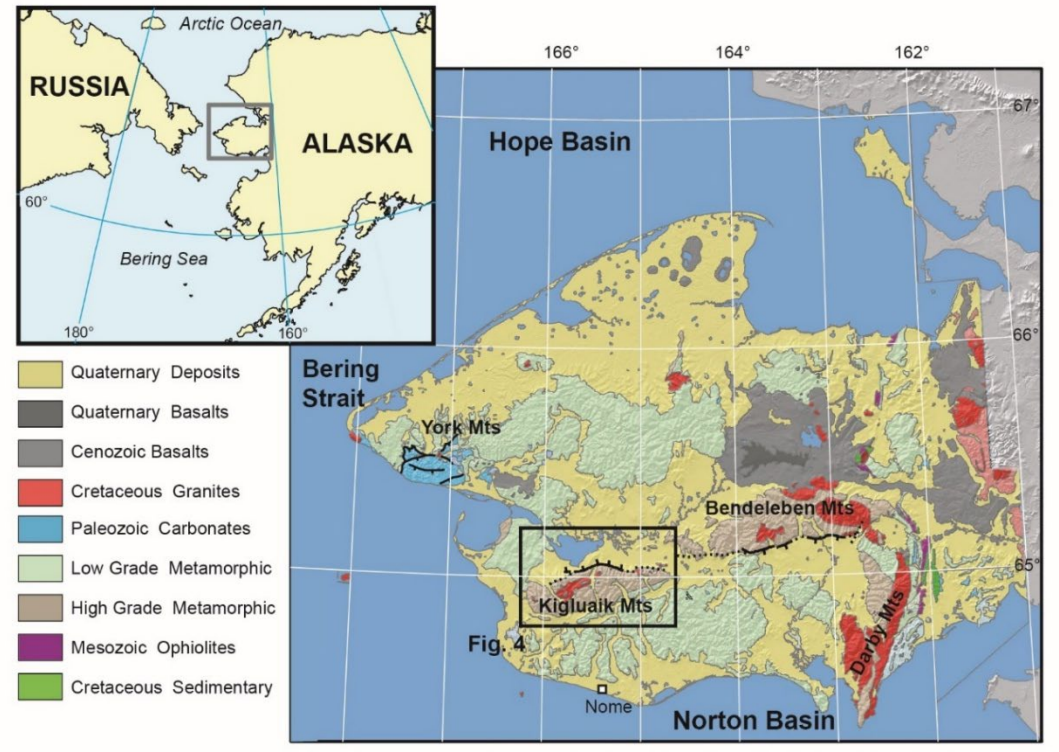

Figure 1: Location and simplified bedrock geologic maps of the Seward Peninsula after Till et al. (2011) and modified from McDannell et al. (2014). Location of Figure 4 shown by black box. Fault symbols are solid where fault scarps are observed on satellite or aerial imagery, and dashed where the faults are inferred. Location of map extent shown in Figure 4 is black rectangle.

Estimates of a ~150˚C PHS reservoir, based on classical geothermometry (Miller et al., 1973; Lofgren, 1983; Liss and Motyka, 1994), sparked drilling campaigns in 1979 and 1983 that yielded maximum downhole temperatures of only 91˚C from a shallow reservoir in a 350 m drilling interval (Kunze and Lofgren, 1983; Lofgren, 1983). These temperatures were not adequate for economic geothermal production at the time. In 2010, PHS exploration resumed with numerous detailed studies (ACEP, 2015) that culminated in 70 geoprobe holes up to 47 m deep and drilling of 8 new wells with the deepest well reaching nearly 400 m depth. Ubiquitous temperature reversals across the well field, with a maximum temperature of 91°C (Benoit et al., 2014a, 2014b), ultimately demonstrated that drilling had not successfully targeted the deeper source of upwelling and no further coordinated geothermal exploration has occurred since.

This study aims to evaluate and refine conceptual models of the PHS geothermal system by integrating new Quaternary mapping, structural analysis, and aqueous GeoT multicomponent geothermometry (Spycher et al., 2014) with existing geophysics and temperature datasets (ACEP, 2015). At least two conceptual models exist for the upflow of hydrothermal fluids at PHS: A) blind faults within the Imuruk basin (e.g., Glen et al., 2014; Benoit, 2014a, 2014b; Miller et al., 2013a, 2013b), and B) the Kigluaik normal fault. We have applied low temperature (U-Th)/He thermochronology along the trace of the Kigluaik normal fault as a pilot study investigating thermochronology as a tool for geothermal exploration. The integrated approach employed in this study provides new insight to test conceptual models of PHS and identify new regional targets for future geothermal exploration programs.

High-resolution thermochronology from rocks along the surface trace of normal faults is a promising means for identifying localities with blind hydrothermal activity. The zircon (U-Th)/He system generally records temperatures around 180°C (e.g., Flowers et al., 2022a) and is used in this study as a background temperature constraint together with existing apatite fission track thermochronology in the Kigluaik Mountains (Dumitru et al., 1995). The apatite (U-Th)/He system is sensitive to short-lived thermal disturbances as low as within the 60-80°C range (e.g., Farley, 2000), and has been observed to display partially reset ages from thermal disturbances related to circulating hydrothermal fluids in fault zones (Berger et al., 2022; Louis et al., 2019; Milesi et al., 2019; MacNamee, 2015; Gorynski et al., 2014; and Hickey et al., 2014). This method is a novel and cost-effective tool for geothermal exploration of normal fault systems like the Kigluaik fault system (example shown in Fig. 2), that would otherwise require costly, high-risk, and environmentally impactful drilling programs to investigate a normal fault for the presence of geothermal activity.

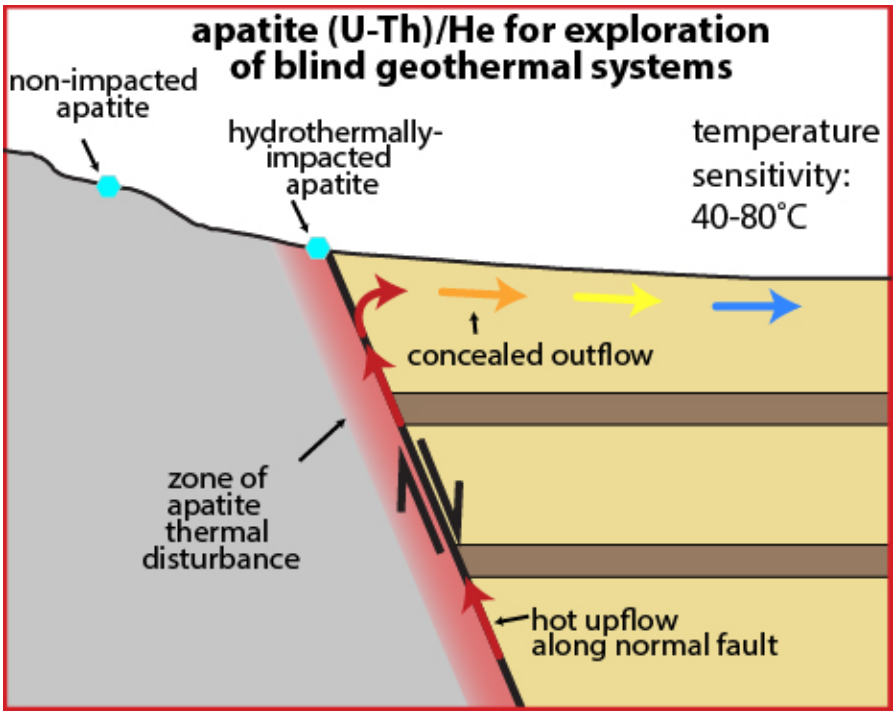

Figure 2: Schematic model for a blind geothermal system and sampling strategy in rocks adjacent to a normal fault to detect hydrothermally impacted apatite using (U-Th)/He thermochronology. Higher temperatures could lead to fully reset apatite (U-Th)/He dates. Figure modified from Richards and Blackwell (2002).

2. Geologic setting

Interior and western Alaska represents an under-studied active tectonic region where north-south crustal shortening to the east transitions to north-south extension in the Bering Sea (Fig. 3). These changing tectonic regimes across the state are driven by regional plate interactions that include subduction and collision of the Yakutat block along Alaska's southern plate boundary (Fig. 3) and the inferred clockwise rotation of a semi-rigid Bering Plate relative to North America (Ruppert, 2008). The Kigluaik Mountains of the Seward Peninsula (Figs. 1 and 4) initially formed as a granite-cored gneiss dome during mid-Cretaceous extension (Amato and Miller, 2002; Amato et al., 1994; Miller et al., 1992). Closely spaced isograds separate high grade, more resistant metamorphic rocks of the gneiss dome from surrounding lower grade (greenschist and locally relict blueschist) and less resistant metamorphic rocks of the Nome Group (Hannula et al., 1995; Amato and Miller, 2004). Although the gneiss dome mostly cooled during the latest Cretaceous to early Cenozoic based on extensive $^{40}Ar/^{39}Ar$ thermochronology and apatite fission track data (Dumitru et al., 1995; Calvert et al., 1999), it is bound on its northern side by a young active normal fault system, here termed the Kigluaik fault system (KFS, Fig. 4), which locally cuts Quaternary glacial moraine deposits.

The KFS, one of the main extensional fault systems in the region, separates the northern range front of the Kigluaik Mountains from the Imuruk Basin along a sharp range front (Fig. 4 and 6b). Post-Wisconsin glacial landforms indicate vertical displacements along the KFS between 4 and 10 m (Hudson and Plafker, 1978; Kaufman et al., 1989; Kaufman, 1986). Although the age of onset of fault slip and the total offset along this active fault are not known with certainty, the mostly

Eocene-Oligocene apatite fission track ages in the core of the dome were interpreted as related to an earlier episode of fault slip during development of the Imuruk Basin which is parallel to bigger transtensional basins, the Hope and Norton Basins, which flank the Seward Peninsula offshore (Dumitru et al., 1995; Tolson, 1987; Worrall, 1991) (Fig. 1). Based on gravity data (Barnes and Hudson, 1977), the depo-center of the Imuruk Basin, which lies to the north of the Kigluaik Mountains (Figs. 1 and 4) was developed as a half-graben in the hanging wall of the bounding KFS. The Bendeleben Mountains contain an active normal fault bounding the southern range front (Fig. 1) and apatite (U-Th)/He and biotite $^{40}Ar/^{39}Ar$ thermochronology record a period of Late Cretaceous-Eocene exhumation (McDannell et al., 2014) with minor post-Miocene reactivation.

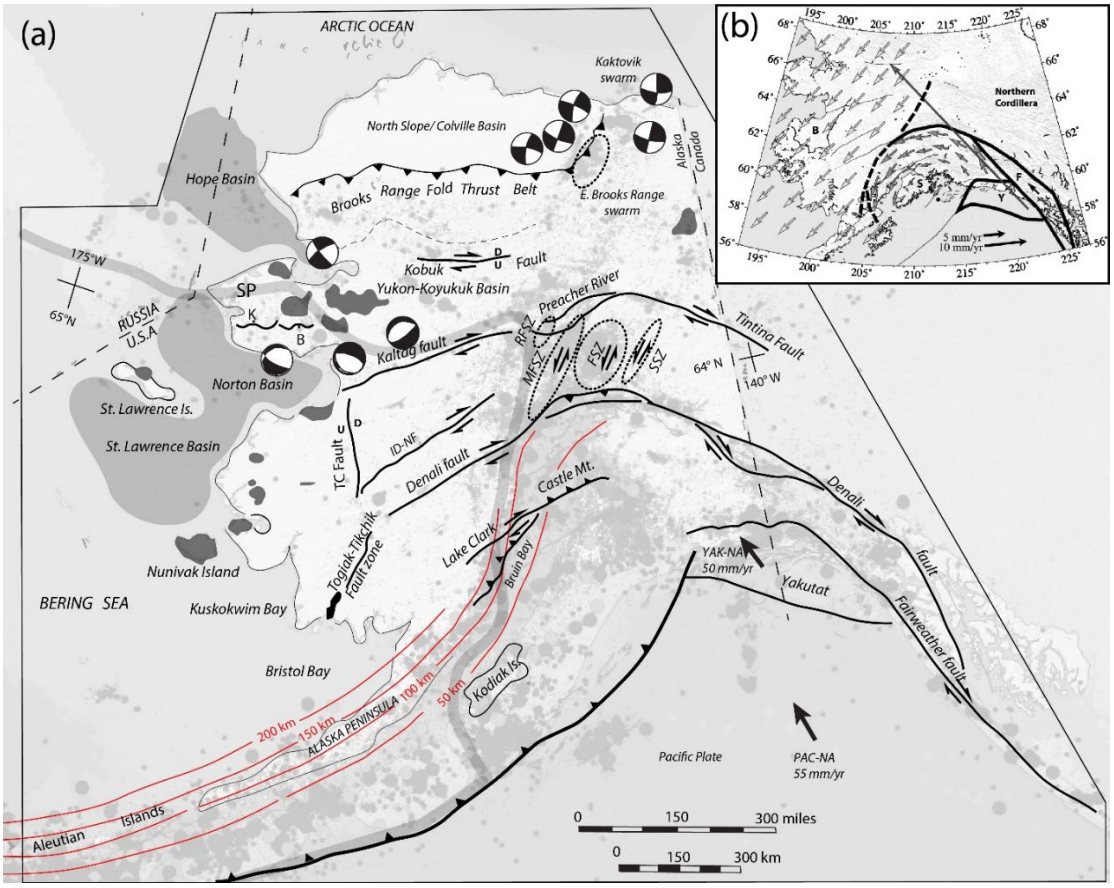

Figure 3: Summary map of active faults and tectonic framework of Alaska. (a) Active faults and contoured depth to Benioff zone from Plafker et al. (1994). Underlay shows earthquakes from 2020 from UAF Alaska Earthquake Center (http://earthquake.alaska.edu/earthquakes). Minton Flats (MFSZ), Fairbanks FSZ and Salsha (SSZ) Seismic Zones have earthquakes indicating left-lateral motion (Ratchkovski and Hansen, 2002; Page et al., 1995). First motions from the Eastern Brooks Range and the Kaktovik earthquake swarms are from Ruppert et al., (2008). Broad grey band is the eastern outline of Mackay and Fujita's (1997) proposed more rigid "Bering block" or plate which was speculated to be rotating clockwise with respect to the rest of Alaska and Russia. PAC-NA and YAK-NA vectors from Elliot et al. (2010). Dark blobs are Cenozoic basalt fields. Abbreviations: SP, Seward Peninsula, K, Kigluaik Mts., B, Bendeleben Mts., TC Fault, I-NF Iditerod-Nixon Fork fault; RFSZ, Rampart seismic zone. (b) Inset shows GPS based block model for the motion of the Bering plate (B) and the adjacent Southern Alaska block (S) which is rotating about the pole shown by black dot and subducting Yakutat terrane (Freymuller et al., 2008), with modelled velocities with respect to North America.

3. Methods and results

Methods employed for evaluating areas of potential upwelling geothermal fluids along the KFS include: 1) Quaternary mapping, 2) structural analysis, 3) campaign-style (U-Th)/He thermochronology, and 4) fluid geochemistry investigations. These methods are used to evaluate whether the KFS represents a structural control for geothermal activity in the region and thus its relationship to PHS. New data presented in this study is then integrated with results of prior studies to present a revised conceptual model for geologic controls of geothermal activity in the region.

3.1 Quaternary mapping

High-resolution DEM from 50 cm areal photogrammetry collected for this study, 2-m Arctic DEM (Porter et al., 2022), and LiDAR (Dannen, pers. commun.) was used to map the KFS in detail (Fig. 4). The KFS is a north-dipping, generally east-west striking, ~ 80 km-long partitioned normal fault system. Recent fault scarps range in height from 4-10 m as measured by offset of Quaternary units to >60 m in recently offset bedrock adjacent to the fault (Fig. 6b). Quaternary units with mapped fault scarps include alluvial fans and glacial moraines associated with the last glacial maximum (27-12.5 ka; Tulenko et al., 2022; Young et al., 2019, Briner et al, 2017; Hamilton et al., 1986; Kaufman et al. 1986).

The KFS contains two mapped portions that are separated near the Cobblestone glacial valley (Fig. 4): the western segment is generally a discrete ENE-WSW-striking fault scarp that bounds the greatest gradient in topography south of Imuruk Lake; the eastern portion is a series of more diffuse, anastomosing, and discontinuous E-W to WNW-ESE striking-scarps that are separated by step-overs that step both to the north and south. A NW-SE striking fault bounding the western edge of the Imuruk Basin, hereafter referred to as the Imuruk fault, intersects the KFS in the western segment near sample JC21-PS30 (Fig. 4), and east of this fault intersection is where the KFS is best developed, most through-going, and contains the greatest change in topographic gradient across the scarp. A concealed NE-SW striking fault identified by gravity surveys (Glenn et al., 2014), referred to as the Pilgrim Springs fault (Fig. 4), intersects the eastern segment of the KFS and projects directly south and adjacent to the surface manifestations of PHS.

The KFS is better developed in the west-central part of the range and does not always cut the last glacial maximum deposits, indicating much of the recent displacement occurred prior to ~15-12.5 ka. The western portion of the range-bounding fault has not been reworked by Quaternary glaciation, whereas the eastern portion of the fault has been extensively reworked. Kaufman (pers. commun., 2019) noted that if the last glacial maximum deposits are >15 ka and the Kigluaik fault cuts them by <10 m, then the Kigluaik fault system slip rate is constrained to be <0.7 mm/yr. The southern range front of the Kigluaik Mountains contains mapped and inferred fault scarps that are generally smaller and less well developed than those bounding the northern range front, indicative of a less to non-active normal fault bounding the southern range front. No offsets of bedrock geology are mapped (Amato and Miller, 2004; Calvert et al., 1999). To the west, the trace of the KFS dies off into colluvium. To the east, the KFS takes a series of northern steps and enters a zone of accommodation (e.g., Faulds and Stewart, 1998) between the KFS and the south dipping Bendeleben normal fault system (Fig. 1) (Till et al., 2011; McDannell et al., 2014).

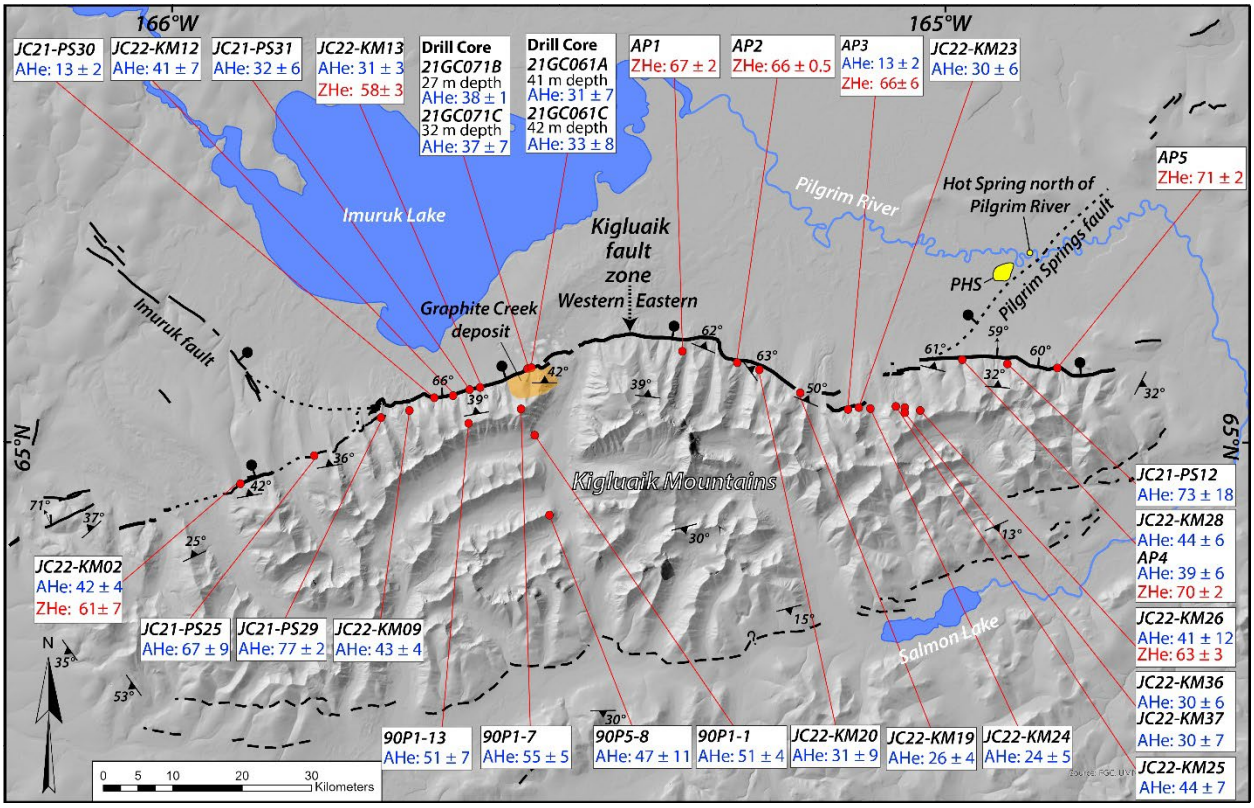

Figure 4: Area map of the Kigluaik Mountains and Pilgrim Hot Springs study area. Mapped Quaternary fault scarps are black lines with balls indicating the down-dip side of fault. Location and extent of Pilgrim Hot Springs and unnamed hot springs north of the Pilgrim River (Daanen., pers. commun.) are shown in yellow. Location of the Graphite Creek deposit shown in orange. Location of thermochronology samples shown as red dots with (U-Th)/He zircon (ZHe; red) and apatite (AHe; blue) cooling ages displayed below sample names (black). Structural data collected in this study supplemented by measurements from Amato and Miller (2004). Western and eastern portions of the KFS separated by dashed black arrow and referenced in text. Map extent shown in Figure 1.

3.2 Structural analysis

Structural analysis was completed on structures measured in outcrop along the KFS and oriented drill core from the Graphite Creek deposit (Fig. 4 and 6). Measurements of structural data were projected onto equal area lower hemisphere projections (Fig. 5). Fault planes in outcrop along the range front generally dip steeply (~50-60°) to the north and slickenlines indicate normal-slip kinematics (Fig. 5a). High quality fault surfaces were limited due to frost heaving and glaciation reworking of most bedrock exposures near the fault. Metamorphic foliation dips moderately to steeply (33-77°) to the north along the KFS with generally strike-perpendicular N-S stretching lineation (Fig. 5b).

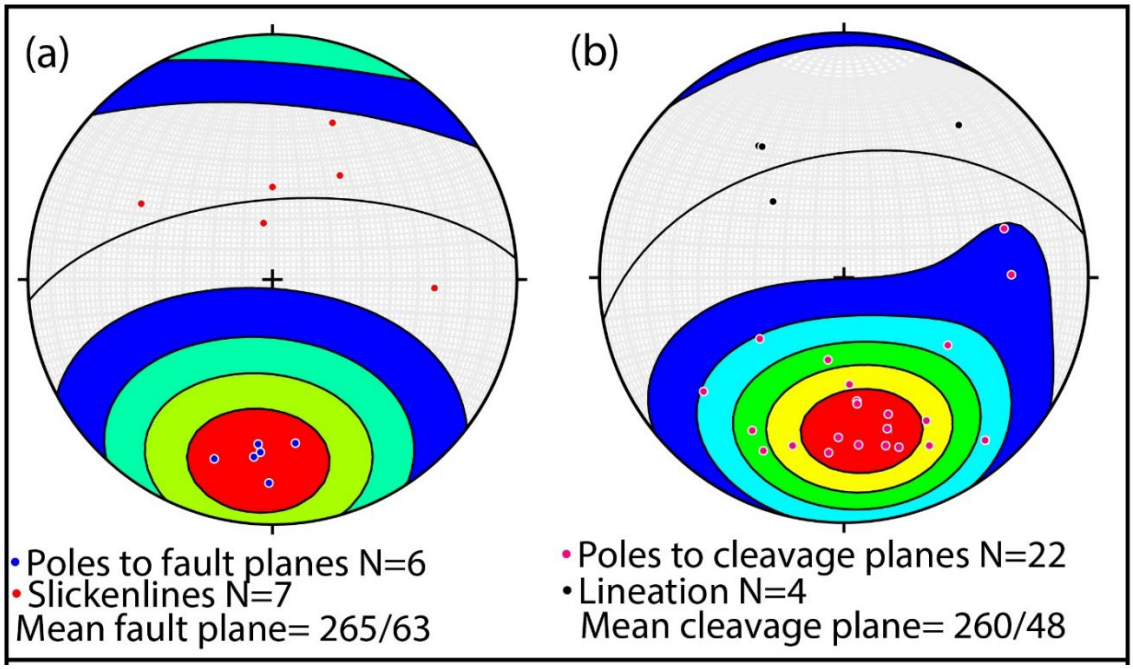

Figure 5: Equal area stereonet projections of structural measurements taken from footwall outcrop exposures of the KFS. (a) Contoured fault poles (blue dots) and slickenlines (red dots). (b) Metamorphic foliation (contoured pink dots) and lineation (black dots). Stereonets generated using Stereonet v. 11.3.1 software (Allmendinger et al., 2012; Cardozo and Allmendinger, 2013).

Distance to the fault plane measured in seven oriented drill holes (locations omitted) taken from the Graphite Creek deposit (e.g., samples 21GC061 and 22GC071 in Fig. 4) were used with the mapped fault scarp to generate three-point problems for estimating the local orientation and dip of the KFS (Table 1). Calculated strike for the local orientation of the fault ranges from 064-083 AZ and dips range from 25-65°, with an average geometry of 072/47° NW. There is some uncertainty in three-point problem fault dip values based on the position of the mapped fault scarp due to erosion and the relatively short depth interval to the fault intersection in drill core.

Table 1: Fault geometry data from oriented drill core at Graphite Creek mineral deposit. Location of drill holes 21GC062 and 22GC071 shown in figure 4.

Drill Hole	Calculated fault strike (AZ)	Calculated fault dip (degree)
18GC023	064	42
18GC024	070	65
18GC025	083	60
18GC026	070	57
21GC061	064	31
21GC062	074	52
22GC071	076	25

3.3 (U-Th)/He thermochronology

Apatite (U-Th)/He thermochronology has a closure temperature between 60-80°C and has been used to detect zones of thermal disturbance associated with upwelling hydrothermal fluids along normal fault systems (Berger et al., 2022; Gorynski et al., 2014; Milesi et al., 2019). This study implements campaign-style apatite (U-Th)/He (AHe) dating of 33 samples along the trace of the KFS and in drill core (Fig. 6) to identify anomalously young cooling dates potentially associated with zones of blind geothermal upwelling (e.g., Fig. 2). Zircon (U-Th)/He (ZHe) dates were collected for 8 samples and used to constrain the higher temperature history as zircon will experience complete loss of radiogenic helium at temperatures greater than 220°C and partial retention of helium down to ~180°C for rapidly cooled samples (Guenthner et al., 2013; Ginster et al., 2019). Sample locations and (U-Th)/He dates are presented in Fig. 4.

(U-Th)/He data were collected at the University of Colorado Thermochronology Research and Instrumentation Laboratory (CU TRaIL) and follow conventions for processing and interpreting (U-Th)/He data outlined in Flowers et al. (2022a, 2022b). (U-Th)/He dates shown in Figure 4 are the average of individual selected grain dates from the sample; uncertainty is the standard deviation of the range of individual dates in a sample. Inverse thermal modeling of each sample was undertaken using HeFTy v. 2.1.4 (Ketcham, 2005).

ZHe average cooling ages from samples collected from bedrock outcrops along the KFS range from Late Cretaceous to Paleocene (71-58 Ma). AHe average dates from samples collected from bedrock outcrops along the KFS range from 73-13 Ma, with most samples distributed between the Paleocene to late Oligocene (50 and 25 Ma). The youngest average AHe dates in the dataset include samples Ap3 (N=2) and JC21-PS30 (N=9), both yielding 13 Ma dates. AHe dates are generally older along the eastern and western ends of the KFS and younger toward the center of the fault. AHe dates also increase with elevation and distance to the south from the KFS.

Four samples of fault rocks intercepted in two drill holes, 21GC061 and 21GC071 (Fig. 4 and 6), from the Graphite Creek mineral deposit were processed for AHe. These samples yield similar Eocene-Oligocene average AHe dates that are observed in outcrop samples. Despite numerous grains representing ‘background’ ages in drill core samples, outliers in 21GC061A (N=11) include one anomalously young ~6 Ma grain and 21GC061C (N=7) which yields 9 and 4 Ma grains. Young grains in drill core samples were excluded from the sample average ages. There is no relationship between the anomalously young ages in drill core samples and effective uranium (eU) or the spherical radius of those grains (Rs) indicative of possible periods of rapid cooling (Flowers et al., 2022 a, b).

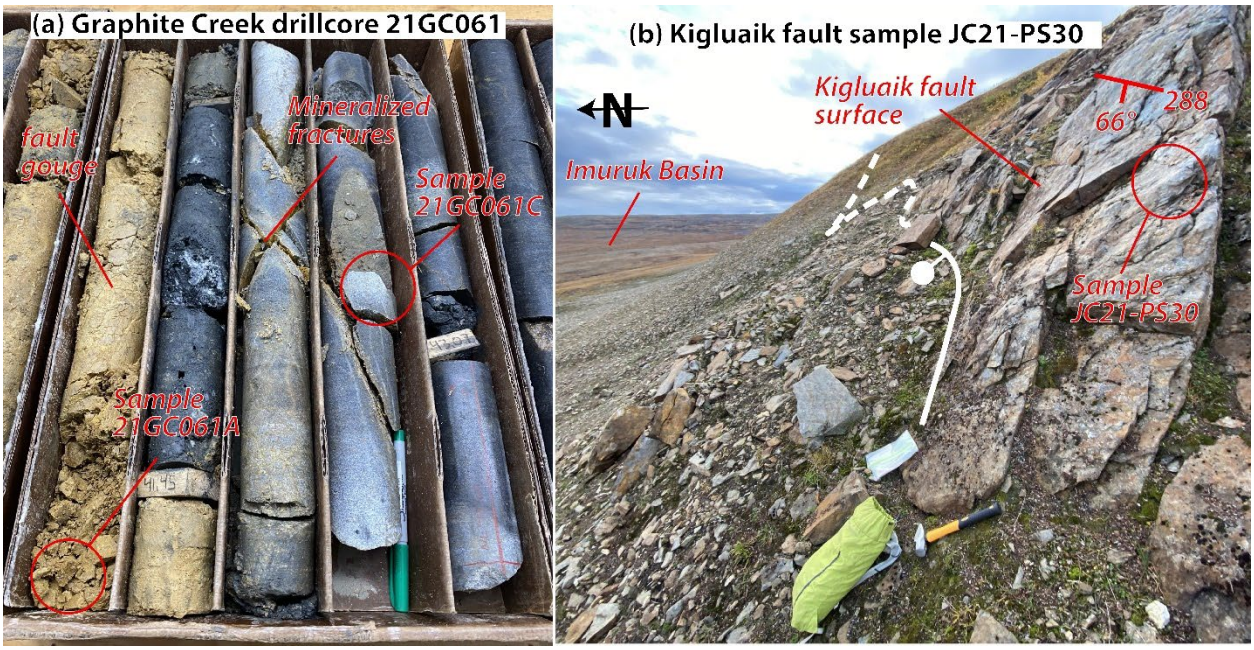

Figure 6: KFS sample photos used for (U-Th)/He thermochronology. Sample localities shown in Fig. 4. (a) Graphite Creek drill core 21GC061 with annotated sample locations, fault gouge, and mineralized fractures. Sharpie (14 cm) for scale. (b) Outcrop sample along KFS scarp at sample JC21-PS30. Hammer (30 cm) for scale. Photo looking east.

3.4 Fluid geochemistry investigations

Five new water samples were collected for this study in the summer of 2021 (Table 2). Water samples were collected from a natural hot spring at PHS, wells PS13-1 and PS13-3, one sample from the Pilgrim River, and a creek in the Kigluaik Mountains. Preliminary GeoT multicomponent equilibria analysis (Spycher et al., 2014) was completed on one legacy water sample of well PS-2 (1979 analysis in Table 2; Liss and Motyka, 1994) which yielded a ~136.5 ± 5°C geothermometer estimate (Fig. 7; Spycher, pers. commun.). Classical geothermometry estimates from sample PS-2 range from 136-170°C and agree with prior estimates.

Table 2: Pilgrim Hot Springs water chemistry. All data from prior to 2021 was copied from ACEP (2015) PHS final report. Values in ppm. ND= not determined.

Sample	Date	T	pH	Na	K	Ca	Mg	Li	B	Si02	HC03	C03	S04	CL	F
--	--	°C	--	ppm	ppm	ppm	ppm	ppm	ppm	ppm	ppm	ppm	ppm	ppm	ppm
Spring (hot)	2021	60	6.94	1370	61.4	511	ND	3.92	2.14	65.4	17.6		ND	3380	5.6
PS13-1	2021	74.9	7.8	890	47.4	335	ND	2.46	ND	61.1	26.6		ND	2100	3.9
PS13-3	2021	77.2	7.5	872	42.2	324	ND	2.41	ND	61	22.5		ND	2090	3.9
PS13-3	2021	77.2	7.2	882	43.1	324	ND	2.49	ND	61.7	21.6		ND	2090	3.4
River (cold)	2021	8	7.56	ND	ND	40.6	ND	ND	ND	ND	73.3		69.3	2.44	ND
Spring (cold)	2021	1.7	6.81	ND	ND	10.6	ND	ND	ND	ND	21.6		11.4	ND	ND
Spring (hot)	1915	70		1590	61	545	7.4			87	21		25	3450	
Spring (hot)	1972	82	6.75	1450	61	530	1.4	4	2.4	100	30.1		24	3346	4.7
Spring (hot)	1982	55	6.8	1660	59	542	1	4.5	2.2	91	36		15	3360	4.3
Spring (hot)	1993	42	6.5	1580	65	569	1.5	4	2.7	86	19		18	3530	4.7
Spring (hot)	1993	55	6.8	1660	59	542	1	4.5	2.2	91	36		15	3360	4.3
Spring (hot)	2012		6.65	1480	62.8	508	0.38	3.6	2	86	14		22	3350	4.6

Spring (hot)	2014	73	6.63	1400	58	460	1	3.4	2.1	80	15			3500	
PS-1	1979	90.5	6.4	1828	75	518	0.9	3.9	2.5	95	16		16	3590	4.8
PS-1	1982	92	7.5	1720	60	511	0.9	4.7	2.3	94	30		19	3420	4.4
PS-1	1993	82	7.1	1560	65	545	0.6	4.2	2.4	90	20		7	3460	5.3
PS-1	2010	79	7.1	1530	61.6	519	1.21	3.5	2.2	83	27.8		14.3	3460	4.5
PS-2	1979	90	6.4	1820	75	516	0.9	3.9	2.3	101	19		15	3540	4.8
PS-2	1982	96	7.3	1510	57	516	0.9	4.7	2.3	92	26		19	3420	4.5
PS-3	1982	75	8	592	25	260	0.4	2	1	60	36		15	1430	1.3
PS-3	1993	65	6.8	1100	43	441	0.6	3.2	1.5	67	27		6	2450	2.9
PS-3	2010	67	7	1140	40.9	412	0.85	2.8	1.7	71	23.7		10.8	2650	3
PS-4	1982	48	8.6	115	4.8	23	0	0.3	0.5	35	80		11	284	0.5
PS-4	1993	45	8.6	146	7.8	98	0.2	0.2	0.2	27	48		1	386	0.3
PS-4	2010	44	8.52	152	5.9	73	0.14	0.5		28	34		9.4	353	0.4
PS-4	2013	44.6	8.47	128	5.5	45	0	0.4	0.2	29	39.9	1.5	9.3	260	0.6
PS-5	1993	32	9.6	36	1.1	2	0.2	0.1	0.6	21	81		5	6	0.5
PS-5	2010	30	9.6	36	1.09	1	0	0.1		20	49.6		5.4	2	0.5
Ml-1	1982	22	9.7	16	0.5	5	0	0.1		21	37		9	5	0.2
Ml-1	1993	31	8.3	29	1.5	23	0.6	0.2	0.1	20	32		10	66	0.2
Ml-1	2010	29	7.8	130	4.4	93	0	0.5		21	25.8		9.5	337	0.2
PS 12-3	2012	65.5	7.52	731	29.9	281	0.78	1.8	1	51	30.6		8.2	1640	1.9
PS 13-1 (open to 1036ft)	2013	70.5	7.51	537	26.1	236	0.4	1.4	0.8	54	25.1		9.3	1300	1.4
PS13-1 (shallow completion)	2013	77	7.27	1090	50.9	370	0.7	2.6	1.5	79	22.8		12.4	2500	3.3
PS 13-1300gpm	2014	79	7.26	1000	35	250		2	1.5	59	18			2500	
PS 13-160gpm	2014	77	7.05	950	37	250		2.1	1.4	67	15			2300	
PS 13-2	2013	71	8.95	124	25	49	0	0.3	0.2	62	39.4	11.1	5.8	265	0.5
PS 13-2 55 gpm	2014	69	7.52	53	3.1	9		0.2	0.1	54	62		5.5	65	
PS 13-3	2013	79	7.27	1070	46.3	373	0.7	2.5	1.4	74	22.1		12.3	2424	3
PS 13-3 60gpm	2014	78	6.97	920	37	280		2.2	1.3	66	16			2200	

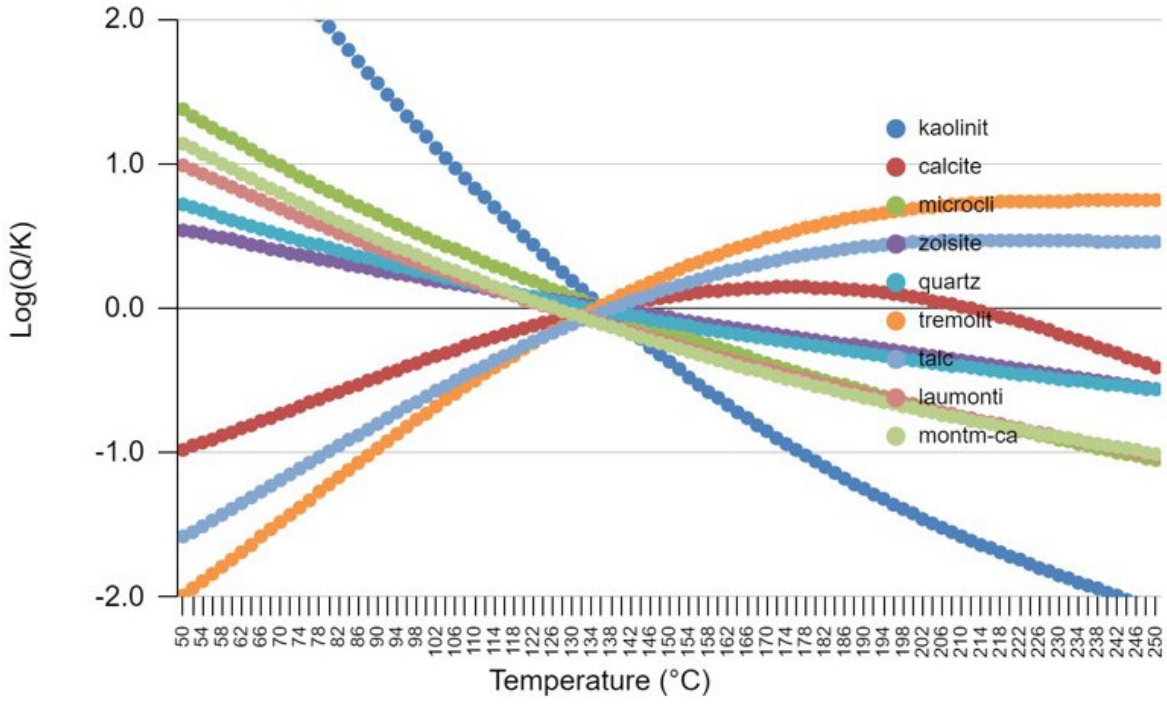

Figure 7: GeoT multicomponent chemical equilibria model results. The modeled minerals attain equilibria under the modeled conditions for Well PS2 from legacy 1979 water chemistry data at 136.5 ± 5°C.

4. Discussion and conclusions

Based on Quaternary mapping and structural analysis, the KFS is an active normal fault accommodating primarily north-south directed extension. Preexisting structures strongly influence the geometry and extent of active faults in the area. The moderately north-dipping KFS straddles the northern extent of the mid-Cretaceous gneiss dome of the Kigluaik Mountains and shares a similar geometry to the associated north-dipping metamorphic foliation (Figs. 4 and 5). Foliation represents a plane of weakness that may localize fault slip as it is optimally oriented in the current stress field (e.g., Donath, 1972).

AHe results primarily capture 40-25 Ma dates along the portions of the KFS that have the most offset (both older offset and recent offset), and dates are older (70-50 Ma) along the eastern and western ends of the fault where there is less total displacement. The younger AHe population is likely related to late Eocene-Oligoene extension in the Bering Sea region that formed the east-west striking basins that bound the Seward Peninsula (Fig. 1 and 3), and which are sub parallel to the onshore KFS and Imuruk Basin (Figs. 1, 3). Similar dates are documented in the adjacent Bendeleben Mountains to the east of the Kigluaik Mountains (McDannell et al., 2014).

The identification of favorable structural settings (e.g., Faulds and Hinz, 2015) along the KFS provides a useful method for guiding geothermal exploration. The updated structural model based on new mapping and structural analysis suggests several favorable structural settings for geothermal activity along the KFS that coincide with samples displaying anomalously young AHe dates. Favorable structural settings include: 1) fault intersections of the KFS with the Imuruk fault and Pilgrim Spring fault, and 2) fault stepovers along the eastern segment of the KFS (Fig. 4).

Anomalously young AHe dates observed in samples AP3 and JC22-PS30 may be indicative of apatite thermal disturbance from hydrothermal fluids. There are numerous thermal histories that could have produced the anomalously young ages, including: 1) complete thermal resetting and degassing of radiogenic He at temperatures above 80°C with subsequent cooling of samples through 60°C at ~13 Ma, and 2) partial degassing of He in apatite that could have occurred at various times (Eocene-Quaternary), durations (days to millions of years), and temperatures (>60°C). Thus, anomalously young AHe dates in a geothermal exploration context are not solely sufficient as direct evidence for the presence of an active geothermal system but can be used as an initial guide for where to focus efforts to test a specific segment of a normal fault for active (or fossil) geothermal activity. Within that context, the segments of the KFS near samples JC22-PS30 and AP3 show potential for hosting (or having hosted) a blind geothermal system.

The eastern segment of the KFS directly adjacent to and up-hydrologic gradient from PHS did not yield any young AHe dates and thus does not provide any indication that the KFS is the structural control for upwelling fluids at PHS. While the lack of young dates does not completely rule out the KFS as a potential structural control for PHS, we favor the conceptual model where the concealed fault within the basin, the Pilgrim Springs fault in Fig. 4, identified by gravity studies (Glenn et al., 2014) is the primary structure controlling upwelling. GeoT multicomponent geothermometry completed in this study yields 136.5°C equilibration estimates and confirms prior classical geothermometry estimates of >130°C (Benoit, 2014a, Miller et al., 1973; Lofgren, 1983;

Liss and Motyka, 1994), which is high enough temperatures for economic energy production from geothermal fluids with sufficient reservoir permeability.

Acknowledgements

Funding for this study was provided by a research grant from the TomKat Center for Sustainable Energy at Stanford University and by Zanskar Geothermal & Minerals, Inc. The authors are indebted to James Metcalf, Rebecca Flowers, Sabrina Kainz and others at the University of Colorado, Boulder TRaIL lab for completing (U-Th)/He analyses. Thanks to Nic Spycher of the Lawrence Berkley National Laboratory for completing GeoT multicomponent geothermometry analyses. This paper was benefited by insightful discussions with Dick Benoit, Darrel Kaufman, Jason Briner, Travis Hudson, and Ronald Daanen. Graphite One, Inc. is thanked for granting access to core from their drilling operations at Graphite Creek. Monika Fleming and Joel Edwards provided support in the field for sample collection. Bering Air provided helicopter support.

REFERENCES

ACEP, 2015, Pilgrim Hot Springs Geothermal Exploration 2010-2014, Final Report. Alaska Center for Energy and Power at the University of Alaska Fairbanks. 842 p.

Allmendinger, R. W., Cardozo, N., and Fisher, D., 2012, Structural geology algorithms: Vectors and tensors in structural geology: Cambridge University Press (book to be published in early 2012).

Cardozo, N., and Allmendinger, R.W., 2013, Spherical projections with OSXStereonet: Computers & Geosciences, v. 51, p. 193 – 205, doi:10.1016/j.cageo.2012.07.021.

Amato, J. M., Miller, E. L., 2004, Geologic map and summary of the evolution of the Kigluaik Mountains gneiss dome, Seward Peninsula, Alaska, in, Gneiss Domes in Orogeny, edited by Whitney, D., Teyssier, C., Siddoway, C. S. Geological Society of America Special Paper 380 p. 295–306.

Amato, J. and Miller, E. L., 2002, Orogenic mass transfer and orthogonal flow directions in extending continental crust: An example from the Cretaceous Kigluaik gneiss dome, Seward Peninsula, Alaska, Geological Society of America Special Paper 360, 133-14

Amato, J. M., J. Wright, P. B. Gans, and Miller, E. L., 1994, Magmatically induced metamorphism and deformation in the Kigluaik gneiss dome, Seward Peninsula, Alaska, Tectonics, 13, 515–527.

Barnes, D. F., Hudson, T., 1977, Bouguer gravity map of Seward Peninsula, Alaska: USGS Open-File Report, series 77-796C. https://doi.org/10.3133/ofr77796C

Briner, J.P., Tulenko, J.P., Kaufman, D.S., Young, N.E., Baichtal, J.F. and Lesnek, A., 2017, The last deglaciation of Alaska. Cuadernos de investigación geográfica: Geographical Research Letters, v. 43, pp.429-448.

Benoit, D., Pike, C., and Holdmann, G., 2014a, The Pilgrim thermal anomaly, Geothermal Resources Council Transactions, Vol. 38.

Benoit, D., Pike, C., and Holdmann, G., 2014b, Fluid-entry temperatures, depths, and water chemistry at Pilgrim Hot Springs, Alaska, Geothermal Resources Council Transactions, Vol. 38.

Berger, A., Egli, D., Glotzbach, C., Valla, P.G., Pettke, T., Herwegh, M., 2022, Apatite low-temperature chronometry and microstructures across a hydrothermally active fault zone. Chemical Geology, v. 588, 120633, https://doi.org/10.1016/j.chemgeo.2021.120633

Berman, M. 2017. Energy costs and rural Alaska out-migration. http://hdl.handle.net/11122/7814.

Calvert, A. T., Gans, P. B. and Amato, J.M., 1999, Diapiric ascent and cooling of a sillimanite gneiss dome revealed by 40Ar/39Ar thermochronology: the Kigluaik Mountains, Seward Peninsula, Alaska. In: Ring, U., Brandon, M. T., Lister, G. S. & Willet, S. D. (eds) Exhumation Processes: Normal Faulting, Ductile Flow and Erosion. Geological Society, London, Special Publications, 154, 205-232.

Case, G.N., Karl, S.M., Regan, S.P., Johnson, C.A., Ellison, E.T., Caine, J.S., Holm-Denoma, C.S., Pianowski, L.S. and Marsh, J.H., 2023. Insights into the metamorphic history and origin of flake graphite mineralization at the Graphite Creek graphite deposit, Seward Peninsula, Alaska, USA. Mineralium Deposita, pp.1-24.

Curewitz, D., and Karson, J.A., 1997, Structural settings of hydrothermal outflow: Fracture permeability maintained by fault propagation and interaction: Journal of Volcanology and Geothermal Research, v. 79, p. 149–168, doi: 10.1016/S0377-0273(97)00027-9.

Donath, F.A., 1972. Effects of cohesion and granularity on deformational behavior of anisotropic rock. *Studies in mineralogy and precambrian geology*, *135*, pp.95-128.

Dumitru, T.A., Miller, E.L., O'Sullivan, P.B., Amato, J.M., Hannula, K.A., Calvert, A.T., and Gans, P.B., 1995, Cretaceous to Recent extension in the Bering Strait region, Alaska: Tectonics, v. 14, no. 3, p. 549–563. http://doi.org/10.1029/95TC00206

Elliott, J. L., Larsen, C. F., Freymueller, J. T., & Motyka, R. J., 2010, Tectonic block motion and glacial isostatic adjustment in southeast Alaska and adjacent Canada constrained by GPS measurements. Journal of Geophysical Research: Solid Earth, 115(B9). https://doi.org/10.1029/2009J B007139

Farley, K.A., 2000, Helium diffusion from apatite: general behavior as illustrated by Durango fluorapatite. Journal of Geophysical Research. vol. 105, p. 2903 – 2914.

Faulds, J. and Hinz, N., 2015, Favorable tectonic and structural settings of geothermal systems in the Great Basin region, western USA: Proxies for discovering blind geothermal systems. In Proceedings World Geothermal Congress, Melbourne, Australia, 19-25 April 2015.

Faulds, J.E., and Stewart, J.H., editors, 1998, Transfer zones and accommodation zones: The regional segmentation of the Basin and Range province: Geological Society of America Special Paper 323, 257 p.

Flowers, R.M., Zeitler, P.K., Danišík, M., Reiners, P.W., Gautheron, C., Ketcham, R.A., Metcalf, J.R., Stockli, D.F., Enkelmann, E., Brown, R.W., 2022A, (U-Th)/He chronology: Part 1. Data, uncertainty, and reporting. GSA Bulletin; 135 (1-2): 104–136. doi: https://doi.org/10.1130/B36266.1

Flowers, R.M., Ketcham, R.A., Enkelmann, E., Gautheron, C., Reiners, P.W., Metcalf, J.R., Danišík, M., Stockli, D.F., and Brown, R.W., 2022B, (U-Th)/He chronology: Part 2. Considerations for evaluating, integrating, and interpreting conventional individual aliquot data: Geological Society of America Bulletin, Special Volume on Reporting and Interpretation of Geochronologic Data, v. 134, https://doi.org/10.1130/B36268.1.

Freymueller, J.T., Woodward, H., Cohen, S.C., Cross, R., Elliot, J., Larsen, C.F., Hreinsdóttir, S., and Zweck, C., 2008, Active deformation processes in Alaska, based on 15 years of GPS measurements, in Freymueller, J.T., Haeussler, P.J., Wesson, R.L., and Ekström, G., eds., Active Tectonics and Seismic Potential of Alaska: American Geophysical Union Geophysical Monograph Series 179,

Ginster, U., Reiners, P.W., Nasdala, L., and Chanmuang, N.C., 2019, Annealing kinetics of radiation damage in zircon: Geochimica et Cosmochimica Acta, v. 249, p. 225–246, https://doi.org/10.1016/j.gca.2019.01.033.

Glen, J.M.G., McPhee, D.K., Bedrosian, P.A., 2014, Geophysical investigations of the geologic and hydrothermal framework of the Pilgrim Springs geothermal area, Alaska, PROCEEDINGS, Thirty-Ninth Workshop of Geothermal Reservoir Engineering Stanford University, Stanford, California, February 24–26 2014, 9 p.

Gorynski, K. E., Walker, J. D., Stockli, D. F., and Sabin, A., 2014, Apatite (U–Th)/He thermochronometry as an innovative geothermal exploration tool: A case study from the southern Wassuk Range, Nevada, Journal of Volcanology and Geothermal Research, v. 270, p. 99–114, https://doi.org/10.1016/j.jvolgeores.2013.11.018.

Guenthner, W.R., Reiners, P.W., Ketcham, R.A., Nasdala, L., and Giester, G., 2013, Helium diffusion in natural zircon: Radiation damage, anisotropy, and the interpretation of zircon (U-TH)/He thermochronology: American Journal of Science , v. 313, p. 145–198, https://doi.org/10.2475/03.2013.01.

Hamilton, T.D., Reed, K.M. and Thorsen, R.M., 1986, Glaciation in Alaska. Alaska Geological Society, Anchorage. Alaska.

Hannula, K.A., Miller, E.L., Dumitru, T. A., Lee, J., Rubin, C. M, 1995, Structural and metamorphic relations in the southwest Seward Peninsula, Alaska: Crustal extension and the unroofing of blueschists. GSA Bulletin 19; 107 (5): 536–553. doi: https://doi.org/10.1130/0016-7606(1995)107<0536:SAMRIT>2.3.CO;2

Haselwimmer, C., Prakash, A., Holdmann, G., 2013, Quantifying the heat flux and outflow rate of hot springs using airborne thermal imagery: Case study from Pilgrim Hot Springs, Alaska, Remote Sensing of Environment, 136, 37-46.

Hickey, K.A., Barker, S.L.L., Dipple, G.M., Arehart, G.B., and Donelick, R.A., 2014, The brevity of hydrothermal fluid flow revealed by thermal halos around giant gold deposits: Implications for Carlin-type gold systems: Economic Geology and the Bulletin of the Society of Economic Geologists , v. 109, p. 1461–1487, https://doi.org/10.2113/econgeo.109.5.1461.

Holcombe, R., 2023, Oriented drill core: measurement, conversion, and QA/QC procedures for structural and exploration geologists: Rod Holcombe/HCOV Global.

Hudson, T., and Plafker, G., 1978, Kigluaik and Bendeleben faults, Seward Peninsula, in Johnson, K.M., ed., The United States Geological Survey in Alaska—Accomplishments during 1988: U.S. Geological Survey Circular 772-B, p. 47–50.

Kaufman, D.S., 1986, Surficial geologic map of the Solomon, Bendeleben, and southern part of the Kotzebue quadrangles, western Alaska: U.S. Geological Survey Miscellaneous Field Studies Map MF-1838-A, 1 sheet, scale 1:250,000.

Kaufman, D.S., 1985, Windy Creek and Crater Creek faults, Seward Peninsula, in Bartsch-Winkler, Susan, and Reed, K.M., eds., The United States Geological Survey in Alaska--accomplishments during 1983: U.S. Geological Survey Circular 945, p. 22-25.

Ketcham, R.A., 2005, Forward and inverse modeling of low-temperature thermochronometry data: Reviews in Mineralogy and Geochemistry , v. 58, p. 275–314, https://doi.org/10.2138/rmg.2005.58.11.\

Liss, S.A., and Motyka, R.J., 1994, Pilgrim Springs KGRA, Seward Peninsula, Alaska: Assessment of fluid geochemistry, Geothermal Resources Council Transactions, v. 18, p. 213–219.

Lofgren, B. E., (Woodward –Clyde), 1983, Geothermal energy development at Pilgrim Springs, Alaska, Phase II: results of drilling testing and resource confirmation April 15, 1983, Report Submitted to State of Alaska Division of Energy and Power Development, 62 p.

Louis, S., Luijendijk, E., Dunkl, I., Person, M; Episodic fluid flow in an active fault. Geology 2019;; 47 (10): 938–942. doi: https://doi.org/10.1130/G46254.1

Mackey, K.G., Fujita, K.; Gunbina, L.V., Kovalev, V. N., Imaev, V.S., Koz'min, B.M., Imaeva, L.P., 1997, Seismicity of the Bering Strait region: Evidence for a Bering block, Geology v. 25, p. 979-982.

MacNamee, A. F., 2015, Thermochronometric investigation of structural evolution and geothermal systems in extensional settings, Dixie Valley, Nevada, (MS thesis). Austin, Texas: University of Texas, Austin. http://hdl.handle.net/2152/32600

McDannell, K. T., J. Toro, J. K. Hourigan, and D. Harris, 2014, Thermochronologic constraints on Late Cretaceous to Cenozoic exhumation of the Bendeleben Mountains, Seward Peninsula, Alaska, Geochem. Geophys. Geosyst., 15, 4009–4023, doi:10.1002/2014GC005424.

Milesi, G., Soliva, R., Moni´e, P., Münch, P., Bellanger, M., Bruguier, O., Bonno, M., Taillefer, A., Mayolle, S., 2019, Mapping a geothermal anomaly using apatite (U/ Th)/He thermochronology in the Tˆet fault damage zone, eastern Pyrenees, France. Terra Nova, v.31, p. 569–576. https://doi.org/10.1111/ter.12429.

Miller, E. L., Calvert, A. T., Little, T. A., 1992, Strain-collapsed metamorphic isograds in a sillimanite gneiss dome, Seward Peninsula, Alaska, Geology v. 20 (6): 487-490.

Miller, T. P., 1994, Geothermal resources of Alaska, in Plafker, G., and Berg, H. C., eels., The Geology of Alaska: Boulder, Colorado, Geological Society of America, The Geology of North America, v. G-1.

Miller, T. P., 1973, Distribution and chemical analyses of thermal springs in Alaska, U. S. Geological Survey Open-file Map 570, scale 1:2,500,000.

Miller, J. K., Prakash, A., Daanen, R., Haselwimmer, C., Whalen, M., Benoit, D., Cumming, W., Clark, A. C., Mager, M., and Holdmann, G., 2013a, Geologic model of the geothermal anomaly at Pilgrim Hot Springs, Seward Peninsula, Alaska, PROCEEDINGS, Thirty-Eighth Workshop on Geothermal Reservoir Engineering, Stanford University, Stanford, CA.

Miller, J. K., Haselwimmer, C., and Prakash, A., 2013b, Investigating low temperature hydrothermal alteration in drill cuttings from Pilgrim Hot Springs, Alaska, using a suite of low cost analytical techniques, Geothermal Resources Council Transactions, Vol. 37, pp. 989 – 995.

Page, R. A., G. Plafker, and H. Pulpan, 1995, Block rotation in east-central Alaska: a framework for evaluating earthquake potential? Geology 23, 629–632.

Plafker, George, Gilpin, L.M., and Lahr, J.C., 1994, Neotectonic map of Alaska, in Plafker, George, and Berg, H.C., eds., The Geology of Alaska: Geological Society of America, 2 sheets, scale 1:2,500,000.

Porter, C., Howat, I., Noh, M., Husby, E., Khuvis, S., Danish, E., Tomko, K., Gardiner, J., Negrete, A., Yadav, B., Klassen, J., Kelleher, C., Cloutier, M., Bakker, J., Enos, J., Arnold, G., Bauer, G., Morin, P., 2022, ArcticDEM – Strips, Version 4.1: Harvard Dataverse, V1. https://doi.org/10.7910/DVN/C98DVS

Ratchovski, N.A., and Hansen, R.A., 2002, New Constraints on Tectonics of Interior Alaska: Earthquake locations, source mechanisms and stress regime, Bull. Seismological Society of America v. 92: 998-1014. https://doi.org/10.1785/0120010182

Richards, M., and Blackwell, D., 2002, A difficult search: Why Basin and Range systems are hard to find: Geothermal Resources Council Bulletin, v. 31, p. 143-146.

Rizzo, A.L., Robidoux, P., Aiuppa, A. and Di Piazza, A.. 2022. 3He/4He Signature of Magmatic Fluids from Telica (Nicaragua) and Baru (Panama) Volcanoes, Central American Volcanic Arc. *Applied Sciences*, *12*(9), p.4241.

Ruppert, N.A., Ridgway, K.D., Freymueller, J.T., Cross, R.C., and Hansen, R.A., 2008, Active tectonics of interior Alaska—Seismology, GPS geodesy, and local geomorphology, in Freymueller, J.T., Haeussler, P.J., Wesson, R.L., and Ekström, G., eds., Active Tectonics and Seismic Potential of Alaska: American Geophysical Union Geophysical Monograph Series, v. 179, p. 109–133. http://doi.org/10.1029/179GM06

Spycher, N., Peiffer, L., Saldi, G., Sonnenthal, E., Reed, M.H., Kennedy, B.M., 2014, Integrated multicomponent solute geothermometry. Geothermics, v. 51, p. 113–123.

Till, A. B., Dumoulin, J.A., Werdon, M.B., Bleick, H. A., 2011, Bedrock Geologic Map of the Seward Peninsula, Alaska, and Accompanying Conodont Data, U.S. Department of the Interior, U. S. Geological Survey.

Tulenko, J. P., Briner, J. P., Young, N E., Schaefer, J. M., 2022, The last deglaciation of Alaska and a new benchmark 10Be moraine chronology from the western Alaska Range, Quaternary Science Reviews, Volume 287, 107549, ISSN 0277-3791, https://doi.org/10.1016/j.quascirev.2022.107549.

Tolson, R. B., Structure and stratigraphy of the Hope Basin, southern Chukchi Sea, Alaska, in Geology and Resource Potential of the Continental Margin of Western North America and Adjacent Ocean Basins, Beaufort Sea to Baja California, Earth Sci. Ser., vol. 6, edited by D.

W. Scholl, A. Grantz, and J. G. Vedder, pp. 59-72, Circum-Pacific Council for Energy and Mineral Resources, Houston, Tex., 1987.

Worrall, D. M., Tectonic history of the Bering Sea and the evolution of Tertiary strike-slip basins of the Bering Shelf, Spec. Pap. Geol. Soc. Am., 257, 120 pp., 1991.

Young, N.E., Briner, J.P., Schaefer, J., Zimmerman, S., Finkel, R.C., 2019, Early Younger Dryas glacier culmination in southern Alaska: Implications for North Atlantic climate change during the last deglaciation: Geology, v. 47, pp. 550-554